3952 *Chem. Mater.* **2010,** *22,* 3952–3960
DOI:10.1021/cm100697b

CHEMISTRY OF MATERIALS
Article

Structure and the Metal Support Interaction of the Au/Mn Oxide Catalysts

Alessandro Longo,*[,†] Leonarda F. Liotta,[†] Gabriella Di Carlo,[†] Francesco Giannici,[‡] Anna Maria Venezia,[†] and Antonino Martorana[†,‡]

[†]*Consiglio Nazionale delle Ricerche, Istituto per lo Studio dei Materiali Nanostrutturati, Sezione di Palermo, Via Ugo La Malfa, 153, I-90146 Palermo, Italy, and* [‡]*Dipartimento di Chimica Inorganica e Analitica "Stanislao Cannizzaro", Università di Palermo,Viale delle Scienze, I-90128 Palermo, Italy*

Received March 8, 2010. Revised Manuscript Received May 26, 2010

Gold catalysts with loading 1 and 10 wt % were prepared by deposition−precipitation method with urea over mesoporous manganese oxide, obtained through a surfactant-assisted procedure by using cetyltrimethylammonium bromide (CTAB), followed by treatment with sulphuric acid. For comparison, Au(10 wt %) was also deposited over commercial CeO_2 and SiO_2 supports. The materials were characterized by XRD and EXAFS at the Mn K and Au L_{III} edges and XPS. Moreover, the analyses were performed on the samples treated under 1%CO/He, at 250 °C for 90 min. The structural and surface results of the as prepared manganese oxide confirmed the formation of γ-MnO_2 along with some amorphous Mn_3O_4 upon treatment of the precursor oxide with sulphuric acid. The CO treatment induces the formation of reduced phases, Mn_3O_4 (Hausmannite) and Mn_2O_3 (Bixbyite). Gold particles have a positive effect in promoting the reduction of manganese oxide and this effect is more pronounced in the Au(10 wt %) catalyst, which exhibits an enhanced CO oxidation activity with respect to both the Au(1 wt %) sample and the metal-free manganese oxide. The higher efficiency of Au(10 wt %) catalyst is attributed to a strong metal−support interaction between gold nanoparticles and support, as demonstrated by the presence of a component Au−O at 2.1 Å in the Fourier transform of the EXAFS signal of both the fresh and the CO-treated samples.

1. Introduction

The oxidation of carbon monoxide is one of the pivotal reactions in heterogeneous catalysis, owing to its application in indoor air cleaning, automotive exhaust treatment, CO_2 lasers, breathing apparatuses, and fuel cells.[1] The catalysts based on supported gold nanoparticles have attracted recent attention because of their exceptionally high activity for low-temperature CO oxidation.[2−4] Different aspects have been studied in order to explain such extraordinary catalytic behavior, including the nature of gold active sites, the influence of support, the preparation method, the preparation conditions, the gold particle size and oxidation state, and the catalyst pretreatment method. Aiming at understanding the influence of these factors, gold nanoparticles have been deposited on various supports, such as Fe_2O_3 CeO_2, MnO_2, MgO, TiO_2, Al_2O_3, ZnO, Co_3O_4, ZrO_2, SnO_2.[5−20]

Among these supports, CeO_2 has been the most extensively investigated for different oxidation reactions, including the water−gas shift and the CO preferential oxidation in the presence of H_2; moreover, ceria is a fundamental component of three way catalysts, due to

*Corresponding author. E-mail: alessandro.longo@cnr.it.

(1) Bond, G. C.; Thompson, D. T. *Catal. Rev. Sci. Eng.* **1999**, *41*, 319.
(2) Bond, G. C.; Louis, C.; Thompson, D. T. *Catalysis by Gold*; Imperial College Press: London, 2006; Vol. *6*.
(3) Su, F. Z.; Liu, Y. M.; Wang, L. C.; Cao, Y.; He, H. Y.; Fan, K. N. *Angew. Chem., Int. Ed.* **2007**, *47*, 334.
(4) Min, B. K.; Friend, C. M. *Chem. Rev.* **2007**, *107*, 2709.
(5) Lin, H. Y.; Chen, Y.-W. *Ind. Eng. Chem. Res.* **2005**, *44*, 4569–4576.
(6) Bamwenda, G. R.; Tsubota, S.; Nakamura, T.; Haruta, M. *Catal. Lett.* **1997**, *44*, 83.
(7) Zanella, R.; Giorgio, S.; Shin, C. H.; Henry, C. R.; Louis, C. *J. Catal.* **2004**, *222*, 357.
(8) Haruta, M.; Tsubota, S.; Kobayashi, T.; Kageyama, H.; Genet, M. J.; Delmon, B. *J. Catal.* **1993**, *144*, 175.
(9) Wolf, A.; Schüth, F. *Appl. Catal., A* **2002**, *226*, 1.
(10) Schubert, M. M.; Hackenberg, S.; Veen, A. C. V.; Muhler, M.; Plzak, V.; Behm, R. J. *J. Catal.* **2001**, *197*, 113.
(11) Schwartz, V.; Mullins, D. R.; Yan, W.; Chen, B.; Dai, S.; Overbury, S. H. *J. Phys. Chem. B* **2004**, *108*, 15782.
(12) Yang, J. H.; Henao, J. D.; Raphulu, M. C.; Wang, Y.; Caputo, T.; Groszek, A. J.; Kung, M. C.; Scurrel, M.; Miller, J. T.; Kung, H. H. *J. Phys. Chem. B* **2005**, *109*, 10319.
(13) Han, Y. F.; Zhong, Z.; Ramesh, K.; Chen, F.; Chen, L. *J. Phys. Chem. C* **2007**, *111*, 3163.
(14) Qian, K.; Huang, W.; Jiang, Z.; Sun, H. *J. Catal.* **2007**, *248*, 137.
(15) Haruta, M. *Catal. Today* **1997**, *36*, 153.
(16) Schubert, M. M.; Kahlich, M. J.; Gasteiger, H. A.; Behm, R. J. *J. Power Sources* **1999**, *84*, 175.
(17) Venezia, A. M.; Pantaleo, G.; Longo, A.; Di Carlo, G..; Casaletto, M. P.; Liotta, F. L.; Deganello, G. *J. Phys. Chem. B* **2005**, *109*, 2821–2827.
(18) Gardner, S. D.; Hoflund, G. B.; Davidson, M. R. *Langmuir* **1991**, *7*, 2140–2145.
(19) Sanchez, R. M. T.; Ueda, A.; Tanaka, K.; Haruta, M. *J. Catal.* **1997**, *168*, 125–127.
(20) Schubert, M. M.; Hackenberg, S.; van Veen, A. C.; Muhler, M.; Plzak, V.; Behm, R. J. *J. Catal.* **2001**, *197*, 113–122.

Published on Web 06/16/2010

its ability of exchanging oxygen with the chemical environment.[21−25] Carrettin et al. reported that the surface of nanocrystalline cerium plays a fundamental role in enhancing the catalytic activity of CeO_2-supported gold catalyst and in particular that the pattern of oxygen vacancies originated by the redox processes involving the Ce^{4+}/Ce^{3+} pair allows effective O_2 adsorption and activation for CO oxidation.[26] Guzman et al. found that the nanocrystalline CeO_2 supplies reactive oxygen in the form of surface η_1-superoxide and peroxide ad species at one-electron defect site on the support and the formation of such reactive species is enhanced by gold, whereas precipitated CeO_2 tends to stabilize oxygen as molecular O_2 and $O^{2\delta-}$.[27−29] Recently, Andreeva et al. suggested that the high activity of gold/ceria catalysts is due to the enhanced electron transfer between defective ceria and partially charged gold particles via oxygen vacancies, with formation of a complex between partially charged gold clusters and the support, so that the oxidation reaction proceeds at the interface between small gold clusters in an intimate contact with ceria.[30] On the other hand, Huang et al. demonstrated that the surface structure or the morphology of ceria markedly affects the dispersion and reducibility of Au/CeO_2 catalysts.[31] Most of the cited studies attribute the activity of ceria-supported Au to a direct interaction between the metal and the support. The extent of such interaction, related to the gold particle size and to the support morphology, would affect the electronic state of the CeO_2 substrate. Although the effective charge of the gold clusters on ceria seems now almost completely clarified, the mechanism of the metal−support interaction is still unraveled and a matter of debate.

Among the supports for Au catalysts, manganese oxide has also recently showed interesting properties in oxidation reactions, likely related to the variable valency of manganese. In a comparative study on ceria and manganese oxide supported gold catalysts for the oxidation of carbon monoxide at low temperature, Chang et al. reported that Au/CeO_2 shows higher catalytic activity for CO oxidation as compared to Au/MnO_2.[32−36] The authors attributed this difference to the coexistence of metallic and oxidized gold species on ceria-based catalyst, whereas only metallic species were recognized on manganese oxide.[32] Despite this daunting result, recently Sinha et al. reported novel mesoporous manganese oxide/nanogold catalyst used for the oxidation of volatile organic compounds (VOC), exhibiting high catalytic performance in the oxidation of ethanol. Also in this case, the metal support interaction was claimed to explain the results.[34] The main effect of the interaction between the gold clusters and the support was to enhance the concentration of oxygen vacancies, thereby promoting the adsorption/dissociation of the VOCs at the gold sites and improving the oxidation reaction.[35] The increase in oxygen vacancies was attributed to a structural change of α-manganese oxide toward a more reduced phase, evidenced by a strong contraction of the Mn−O first shell coordination number. Then, it is evident that a careful structural characterization is essential to rationalize the mechanism of metal−support interaction as a function of the potential structural changes of the support.

In this work, aiming at finding a direct evidence of the interaction between gold and manganese oxide, gold (1 and 10 wt %) was deposited on MnO_2 and also on CeO_2 and SiO_2 for comparison reasons. The choice of high (10 wt %) Au loading was motivated byan expected higher metal−support interaction at higher metal content. The materials were characterized by XRD, EXAFS at the Mn K edge and Au L_{III} edge, and by XPS. The analyses were performed on the "as-prepared" and on "CO-treated" samples. The effect of gold on the support redox property was evaluated by performing reduction treatments, under CO atmosphere, on the bare supports and on the corresponding gold catalysts. Possible correlations between structural modification and CO oxidation mechanism are discussed.

2. Experimental Section

2.1. Samples. The synthesis of manganese oxide (from now on, sample A) was carried out through a surfactant-assisted procedure by using cetyltrimethylammonium bromide (CTAB).[34] To obtain mesoporous γ-MnO_2 (sample B), sample A was treated with H_2SO_4 (10M) aqueous solution for 30 min under stirring, and then filtered and washed several times with water until no sulfate ions were detected by the $Ba(NO_3)_2$ test. After being dried at 105 °C overnight, the final mesoporous oxide with specific surface area of 287 m^2/g was obtained.

Gold catalysts, with nominal loading of 1 and 10 wt %, were prepared by deposition-precipitation method with urea over the B sample. Au (10 wt %) was also deposited on commercial CeO_2 (surface area = 79 m^2/g) and commercial SiO_2 (surface area = 560 m^2/g). Typically, 1 g of support was added to 100 mL of an aqueous solution containing $HAuCl_4$ (5×10^{-4} M) and urea (urea/Au = 100, molar ratio). The suspension was kept under

(21) Trovarelli, A. *Catalysis by Ceria and Related Materials*; Catalytic Science Series; Imperial College Press: London, 2002; Vol. *2*.
(22) Heck, R. M.; Farrauto, R. J. *Catalytic Air Pollution Control*; Wiley Inter-Science: New York, 2002.
(23) Tabakova, T.; Boccuzzi, F.; Manzoli, M.; Sobczak, J. W.; Idakiev, V.; Andreeva, D. *Appl. Catal., A* **2006**, *298*, 127–143.
(24) Trovarelli, A. *Catal. Rev. Sci. Eng*. **1996**, *38*, 439–520.
(25) Lai, S. Y.; Qiu, Y.; Wang, S. *J. Catal*. **2006**, *237*, 303–313.
(26) Carrettin, S.; Concepcion, P.; Corma, A.; Lopez Nieto, J. M.; Puntes, V. F. *Angew. Chem., Int. Ed*. **2004**, *43*, 2538–2540.
(27) Guzman, J.; Gates, B. C. *J. Am. Chem. Soc*. **2004**, *126*, 2672–267.
(28) Guzman, J.; Carrettin, S.; Corma, A. *J. Am. Chem. Soc*. **2005**, *127*, 3286–3287.
(29) Guzman, J.; Carrettin, S.; Fierro Gonzalez, J. C.; Hao, Y.; Gates, B. C.; Corma, A. *Angew. Chem*. **2005**, *117*, 4856–4859.Angew. Chem., Int. Ed. **2005**, *44*, 4778 −478.
(30) Andreeva, D.; Ivanov, I.; Ilieva, L.; Sobczak, J. W.; Avdeev, G.; Petrov, K. *Top. Catal*. **2007**, *44*, 173–182.
(31) Huang, X.; Sun, H.; Wang, L.; Liu, Y.; Fan, K.; Cao, Y. *Appl. Catal., B* **2009**, *90*, 224–232.
(32) Akolekara, D. B.; Bhargavaa, S. K.; Foranb, G.; Takahashi, M. *J. Mol. Catal., A* **2005**, *238*(1−2), 78–87.
(33) Chang, L.; Sasirekha, N.; Rajesh, B.; Chen, Y. W. *Sep. Purif. Technol*. **2007**, *58*, 211–218.
(34) Sinha, A. K.; Suzuki, K.; Takanara, M.; Azuma, H.; Nonaka, T.; Fukumoto, K. *Angew. Chem., Int. Ed*. **2007**, *46*, 2891–2894.
(35) Sinha, A. K.; Suzuki, K.; Takahara, M.; Azuma, H.; Nonaka, T.; Suzuki, N.; Takahashi, N. *J. Phys. Chem. C* **2008**, *112*(41), 16028–16035.
(36) Wang, L. C.; Liu, Y.-M.; Chen, M.; Cao, Y.; He, H. Y.; Fan, K.-N *J. Phys. Chem. C* **2008**, *112*, 6981–6987.

stirring for 16 h at 80 °C, in order to favor urea decomposition leading to a gradual rise in pH until ~7. The solids were then filtered, washed with water until no chloride ions were detected by the $AgNO_3$ test and dried in air at 100 °C overnight. The effective Au loading in the samples, determined by ICP-AES technique using ICP Varian Vista MPX instrument, corresponded for the 1 wt % loaded to the nominal one, whereas for the 10 wt % ones was equal to 8.6 wt % for both catalysts, supported over γ-MnO_2 and CeO_2. In the case of silica, the real gold loading corresponded to 3 wt %.

Portions (200 mg) of sample B and of the Au (1,10 wt %) catalysts over manganese oxide, ceria, and silica were fluxed with 1%CO/He (50 mL/min) at 250 °C for 90 min, and then cooled to room temperature under pure He. These treatments were carried out with a Micromeritics Autochem 2910 apparatus connected to a mass quadrupole (Thermostar, Balzers) and an IR analyzer (ABB, Uras 14) for monitoring the CO conversion and CO_2 formation. To ascertain any possible effect induced by the thermal treatment at 250 °C, we also treated a portion of sample B at 250 °C for 90 min under pure He (50 mL/min). This sample is labeled hereafter as C, whereas sample D is obtained from sample B after CO treatment; the gold catalyst Au 10 wt % supported on B after CO treatment is labeled as E. All supports and catalysts not subjected to thermal treatments in gas flux are tagged "as-prepared".

2.2. XRD. Powder X-ray diffraction (XRD) patterns were recorded at room temperature in Bragg−Brentano parafocusing geometry using a Bruker D5000 diffractometer, equipped with a Cu K_α anode and a graphite monochromator on the diffracted beam. The XRD data was collected on the 10−90° 2θ range. To achieve good counting statistics, we chosen long counting times (20 s per step). Rietveld refinement on the XRD data were analyzed according to the using the GSAS program.[37]

2.3. EXAFS Analysis. X-ray absorption spectra were recorded at the Au L_{III}-edge (11.920 keV) and Mn K-edge (6.539 keV) at the BL 11.1 beamline of ELETTRA Sincrotrone Trieste, operating at an energy of 2.4 GeV with a 130 mA storage ring current. The beamline was equipped with a Si (111) double crystal monochromator with energy resolution 2×10^{-4}. In addition to catalyst samples, EXAFS spectra were also acquired for Au foil, as internal standard reference for the energy calibration, and for $AuCl_3$ and Mn foil, as structural references for the samples. EXAFS measurements were performed in transmission mode by using two ionization chambers filled with a N_2/Ar mixture at different composition for the incident I_0 and transmitted I_1 beam, respectively. The samples were crushed by grinding in a mortar, pressed in self-supporting wafers, and mounted in a sample holder suitable for EXAFS data collection. To avoid support reoxidation and/or ambient oxygen absorption on the gold particles, wer prepared the pellets of the samples treated in CO under He flux, coated them with kapton tape and then mounted them in the sample holder.

The measurements were performed at liquid-nitrogen temperature (LN) to limit the thermal disorder effects that damp the EXAFS oscillations, thus allowing the collection of high-quality data, well above the instrumental noise, in a wide range of photoelectron wave vector magnitude. Data extraction and EXAFS analysis were carried out by the GNXAS package.[38,39]

(37) Larson, A. C.; Von Dreele, R. B. *Los Alamos National Laboratory Report LAUR* **2000**, 86–748.
(38) Filipponi, A.; Di Cicco, A.; Natoli, C. R. *Phys. Rev. B* **1995**, *52*, 15122.
(39) Filipponi, A.; Di Cicco, A. *Phys. Rev. B* **1995**, *52*, 15135.

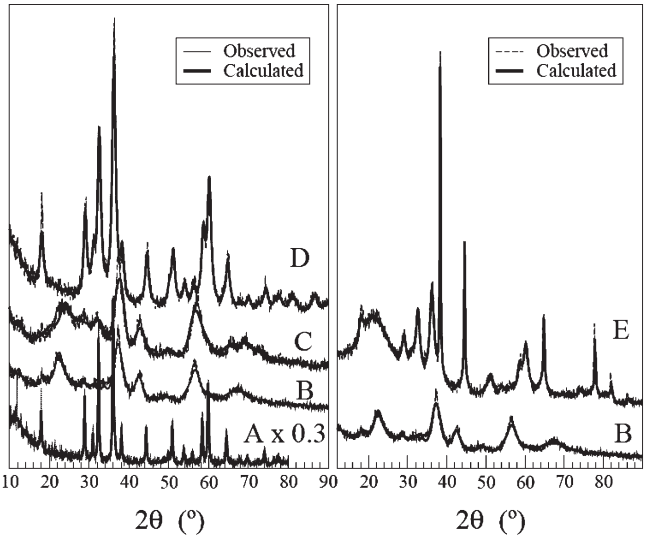

Figure 1. (Left panel) Experimental and calculated XRD patterns of: (A) as-prepared manganese oxide; (B) sample A after H_2SO_4 treatment; (D) sample B after treatment under 1%CO/He, at 250 °C for 90 min. (Right panel) Experimental and calculated XRD patterns of: (B) mesoporous γ-MnO_2; (C) sample B after treatment at 250 °C for 90 min under pure He; (E) Au(10 wt %) catalyst supported over B after treatment under 1%CO/He at 250 °C for 90 min.

2.4. XPS. The X-ray photoelectron spectroscopy analyses were performed with a VG Microtech ESCA 3000 Multilab spectrometer, using the unmonochromatized Al Ka source (1486.6 eV) run at 14 kV and 15 mA. Survey spectra were collected at a constant pass energy of 50 eV, individual peak energy regions were collected at a constant pass energy of 20 eV. Samples were mounted on a stub holder using double-sided adhesive tape. The C 1s peak, set at 285.1 eV, arising from adventitious carbon, was used as reference for the binding energy values. Differential surface charging was ruled out by checking the reproducibility of XPS results in repeated scans under different X-ray exposures. Analyses of the peaks were performed with the software provided by VG, based on nonlinear least-squares fitting routine using a weighted sum of Lorentzian and Gaussian component curves after background subtraction according to Shirley and Sherwood.[40] Atomic concentrations were calculated from peak intensity with the standard set of VG Escalab sensitivity factors. The binding energy values are quoted with a precision of ±0.15 eV and the atomic percentage with a precision of ±10%.

3. Results

3.1. XRD. In Figure.1 the experimental and calculated XRD patterns of the manganese oxide and of the supported gold catalysts are shown. As determined by Rietveld analysis, the precursor Mn oxide (sample A) is Hausmannite, Mn_3O_4, (tetragonal, *I*41/*amd*, No. 141). In Table 1, the refined structural parameters and the agreement factors are reported. The treatment with sulfuric acid induces a deep structural change in the A sample, leading to the formation of γ-MnO_2 (sample B). By inspection of Figure 1, it is evident that the γ-phase exhibits nanostructured features as witnessed by the very

(40) Sherwood, P. M. A.; Briggs, D.; Seah, M. P. *Practical Surface Analysis*; Wiley: New York, 1990; Vol. *181*.

Table 1. XRD Results from Rietveld Refinement[a]

sample	phase fraction	*a* (Å)	*b* (Å)	*c* (Å)	α (Å)	*β* (Å)	*γ* (Å)	phase fraction	*a* (Å)	*b* (Å)	*c* (Å)	α (deg)	*β*	*γ*	R (%)
A	*I* 41/*amd* (Hausmannite) 100%	5.776(7)	5.776 (7)	9.43(1)	90	90	90								5.2
B	*C* 12/*m 1* (γ-MnO_2) 100%	9.86(2)	5.709(7)	4.884(9)	90	107.5(5)	90								7.6
C	*C* 12/*m*1 (γ-MnO_2) 100%	14.01(3)	2.887(3)	4.367(5)	90	88.3(3)	90								5.2
D	*I* 41/*amd* (Hausmannite) 100%	5.756(7)	5.756 (7)	9.40(1)	90	90	90								6.8
E	*I* 41/*amd* (Hausmannite) 93.(5) %	5.762(7)	5.762(7)	9.36(1)	90	90	90	$Fm\bar{3}m$ (gold) 7.(3) %	4.0682(2)			90	90	90	5.5

[a]For every sample, the phase composition is reported. *a*, *b*, and *c* are the lattice constants (Å), and α, *β*, and *γ* are the crystallographic angles. Sample A, manganese oxide calcined at 500 °C for 4 h; Sample B, sample A after H_2SO_4 treatment; Sample C, sample B after thermal treatment under He at 250 °C; Sample D, sample B after CO treatment at 250 °C; Sample E, sample B after Au (10 wt %) deposition and CO treatment at 250 °C. The *R* factor is the agreement obtained with the Rietveld refinement.

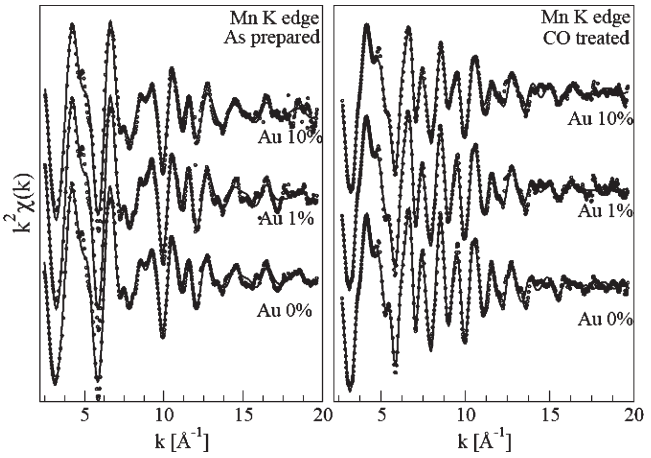

Figure 2. Extracted EXAFS signals (circles) and calculated spectra (line) fitted to the data for as prepared samples (right panel) and after CO treatment at 250 °C (left panel).

broad peaks. It is worth of note that, to carry out the Rietveld refinement of sample B, an important background component was needed, suggesting that the sulfuric acid treatment induces the formation of a large amount of an amorphous phase. After reduction with CO, the Hausmannite structure is recovered, both in the bare support and in the Au catalyst (Figures 1 D and 2 E).

Looking at the pattern of the B sample fluxed at 250 °C under He (Figure 1C), it can be observed that the mere thermal treatment does not induce any structural transformation, only producing a slight increase in crystallite size. Because of the large amount of gold (10% weight) used in the synthesis of sample E, the presence of gold metal clusters of about 8 nm can be detected.

3.2. Mn−K Edge Analysis. On the basis of the XRD results (Table 1), the Mn−K edge EXAFS spectra of the "as prepared" samples were analyzed according to the γ-MnO_2 phase. This phase is constituted by a double chain of MnO_6 corner sharing octahedra, whereas the adjacent chains have the octahedral corner in common. The whole structure is an intergrowth of these arrangements with noticeable stacking faults which make the structure extremely disordered.[41] For the EXAFS signals generation, six Mn−O mean distances at 1.90 Å, two mean distances Mn^{4+}−Mn^{4+} at 2.84 Å (relative to the edge sharing), and eight mean distances Mn^{4+}−Mn^{4+} centered at 3.44 Å (relative to the corner sharing octahedra), were used. However, the agreement between the observed signal and the calculated EXAFS was rather poor, suggesting that the γ-MnO_2 distances are not sufficient to describe the local environment of the Mn cations. The details of this EXAFS analysis are reported in the Supporting Information. The unsatisfactory agreement was ascribed to small crystallites of unreacted Hausmannite, which represents the main crystallographic phase of the support before the treatment with sulfuric acid. The composition of Hausmannite can be represented as $Mn^{2+}Mn^{3+}{}_2O_4$, the crystal structure being a spinel-type cubic close packing of oxide ions, with tetrahedral sites occupied by Mn^{II} and octahedral cavities by Mn^{III} cations. These latter sites present a noticeable Jahn−Teller distortion;[48] then, two M^{III}−O distances relative to the octahedral surrounding (R_1 = 1.94 Å, CN = 4, R_2 = 2.29 Å, Cn = 2) and one Mn^{II}−O distance (R_3 = 2.014 Å, CN = 4) for the tetrahedral cavity are included in the EXAFS model. Three higher shells of Hausmannite relative to Mn^{3+}−Mn^{3+} (R_4 = 2.889 Å, CN = 2), Mn^{2+}−Mn^{3+} (R_5 = 3.432 Å, CN = 8), and Mn^{3+}−Mn^{3+} (R_6 = 3.117 Å, CN = 4) distances were also taken into account. The results of the EXAFS analysis, which includes the two crystallographic arrangements, are reported in Table 2, and shown in Figures 2 and 3 (left panel). In the analysis, the coordination numbers were kept fixed; therefore, 14 structural parameters, including one parameter to weight the different crystallographic arrangements and E_0, were needed. According to the Nyquist criterion, and assuming that the EXAFS data are significant over the 1−5 Å range, the number of independent parameters n_{ind} ($n_{ind} = 2(\Delta K)(\Delta R)/\pi + 2$) is nevertheless low.

The two "as-prepared" gold catalysts (Au 1 and 10 wt %) were analyzed using the same approach. Sample B and the two gold catalysts (Au 1 and 10 wt %) were treated with CO flux as described in the Experimental Section. The detailed analysis of the CO-treated Au 10 wt % catalyst, sample E, is reported in Figure 3 (right panel). Contrary to the XRD results, the Hausmannite structure for sample E did not allow a good agreement between experimental and calculated EXAFS data. An improved result is obtained by using both, the α-Mn_2O_3 (cubic, $Ia\bar{3}$, No. 206) and the

(41) Schilling, O.; Dahn, R. *J. Appl. Crystallogr.* **1998**, *31*, 396–406.

Table 2. EXAFS Analysis Relative to Mn K-Edge of As-Prepared Samples[a]

	As-prepared Sample B	As prepared 1 wt % Au/γ-MnO_2	As prepared 10 wt % Au/γ-MnO_2	Theoretical Values
E_o	6548.(4)	6551.(3)	6551.(2)	6551.
fraction of hausmannite (%)	24(2)	29(2)	37(2)	
R_{1_H}	1.805(5)	1.804(5)	1.808(5)	1.9320
σ_{1_H}	0.0044(2)	0.0070(2)	0.0040(3)	
R_{2_H}	2.014(5)	2.013(5)	2.014(5)	12.014
σ_{2_H}	0.0044(2)	0.0040(2)	0.0040(3)	
R_{3_H}	2.345(5)	2.337(5)	2.326(5)	2.2837
σ_{2_H}	0.0044(2)	0.004(6)	0.004(6)	
θ_{1_H}	102.(5)	101.(5)	102.(5)	95.0
	R = 3.121	R = 3.125	R = 3.121	R = 3.1232
θ_{2_H}	103.(5)	107.(10)	107.(8)	95.58
	R = 3.449	R = 3.4423	R = 3.4423	R = 3.4350
θ_{3_H}	95.(5)	96.(5)	85.(5)	96.58
	R = 2.828	R = 2.856	R = 2.87	R = 2.8846
fraction of γ-MnO_2 (%)	76(2)	71(2)	63(2)	
σ_{1_γ}	0.0054(2)	0.0040(2)	0.0040(3)	
θ_{1_γ}	99.(5)	99.(5)	98.(5)	96.0
	R = 3.121	R = 3.125	R = 3.121	R = 3.1232
θ_{2_γ}	130.(5)	131.(10)	131.(8)	129
	R = 2.887	R = 2.887	R = 2.887	R = 3.4350

[a] The values of the coordination numbers were fixed to the theoretical values: $N_1 = 4$, $N_2 = 2$, $N_3 = 2$. S_0^2 was fixed to 0.74. Distances in Å, Debye−Waller factors in Å^2, angles in degrees. The errors of the fitting parameters are reported in parentheses.

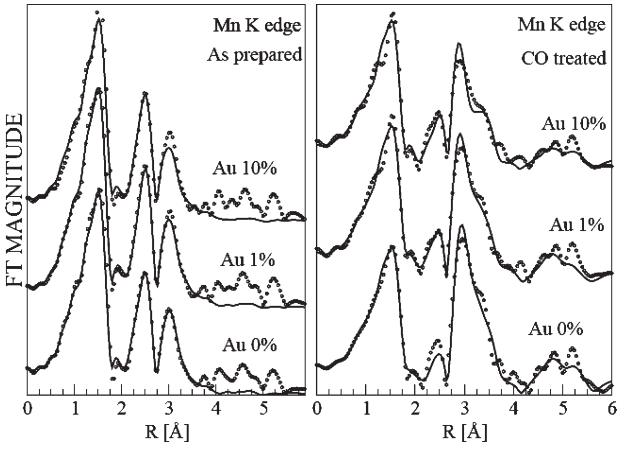

Figure 3. Fourier transform (uncorrected for phase shift) magnitude of the EXAFS signals (circles) and calculated spectra (line) fitted to the data for as prepared samples (right panel) and after CO treatment at 250 °C (left panel).

Table 3. EXAFS Analysis Relative to Mn K-Edge of CO-Treated Samples; Results of the Bixbyite Structure[a]

	sample D	1 wt % Au/ γ-MnO_2 (CO-treated)	sample E (10 wt % Au/γ-MnO_2)	theoretical Values
fraction of bixbyite (%)	62(3)	54(3)	49(3)	
E_0	6551.(2)	6549.(2)	6552.(2)	6551
R_{1_B}	1.888(2)	1.869(2)	1.891(2)	1.8987
σ_{1_B}	0.007(3)	0.0011(3)	0.0015(3)	
θ_{1_B}	118.(4)	118.(5)	118.(5)	118
	R = 3.11	R = 3.11	R = 3.11	R = 3.11
θ_{1_B}	106.(4)	108.(5)	107.(5)	106
	R = 3.511	R = 3.519	R = 3.516	R = 3.511

[a] The values of the coordination numbers were fixed to the theoretical values $N_1 = 4$, $N_2 = 2$, $N_3 = 2$, and $N_1 = 2$, $N_2 = 2$, $N_3 = 2$, $N_3 = 6$, for Bixbyite and Hausmannite, respectively. S_0^2 was fixed to 0.74. Distances in Å, Debye−Waller factors in Å^2, angles in degrees. The errors of the fitting parameters are reported in the parentheses.

Hausmannite phases. The details are reported in the Supporting Information file. To better discriminate the features of the two different structural contributions, the calculated EXAFS signal was extended up to 5.71 Å, so that the higher shells of both phases were taken into account. On the whole, 17 free parameters, 4 for α-Mn_2O_3, 11 for Mn_3O_4, and 2 accounting for the E_0 and the relative weight of the two phases, were needed. The results of EXAFS, are summarized in Tables 3 and 4, respectively, and are shown in Figures 2 and 3 (right panel).

As indicated in Table 4, the more reduced Hausmannite phase increases with Au loading, from 38(3)% in the case of sample D (only support) to 51(3)% for sample E (Au 10 wt % catalyst), suggesting that from a structural point of view the reduction process is sensitive to the Au particles content.

3.4. Au L_{III} Edge. To investigate the possible interaction between gold and support, the EXAFS spectra were recorded at the Au L_{III} edge. Spectra of "as-prepared" Au (10 wt %)/γ-MnO_2 and "after CO treatment" were recorded. For comparison reasons, two gold catalysts, one supported over ceria, a reducible oxide well-known for giving rise to SMSI, and another one supported over inert silica, were analyzed. In Figures 4 and 5, the extracted EXAFS signals and calculated spectra are displayed for both "as-prepared" (left panel) and CO-treated Au (10 wt %) catalysts (right panel). The Au foil was also analyzed as a reference. Table 5 summarizes the EXAFS results of the above catalysts.

The components and the overall calculated and observed EXAFS patterns are shown for the CO treated 10% Au/γ-MnO_2 catalyst in Figure 6 (the FT's are reported in the support information). In the left panel, a Au−O component is included that, as indicated by the residual, is indeed necessary to achieve a good fitting. The corresponding presence of a peak at around 2.1 Å in the

Table 4. EXAFS Analysis Relative to Mn K-Edge of CO-Treated Samples; Results of the Hausmannite Structure[a]

	sample D	1 wt % Au/γ-MnO_2 (CO-treated)	sample E (10 wt % Au/γ-MnO_2)	theoretical values
fraction of Hausmannite (%)	38(3)	44(3)	51(3)	
R_{1_H}	1.913(5)	1.911(5)	1.903(5)	2.889
σ_{1_H}	0.004(3)	0.0042(5)	0.0042(5)	
R_{2_H}	2.343(7)	2.356(7)	2.354(7)	3.570
σ_{2_H}	0.006(9)	0.0400(9)	0.0400(9)	
R_{3_H}	2.083(7)	2.072(7)	2.067(7)	3.570
σ_{2_H}	0.006(9)	0.0400(9)	0.0400(9)	
θ_{1_H}	95.(5)	96.(5)	85.(5)	96.58
	R = 2.828	*R = 2.856*	*R = 2.87*	*R = 2.8846*
θ_{2_H}	100.(5)	101.(5)	102.(5)	95.0
	R = 3.121	*R = 3.125*	*R = 3.121*	*R = 3.1232*
θ_{3_H}	117.(5)	117.(10)	117.(8)	95.58
	R = 3.449	*R = 3.4423*	*R = 3.4423*	*R = 3.4350*
θ_{4_H}	116.(7)	118.(7)	121.(7)	117.
	R = 5.184	R = 5.179	R = 5.300	*R = 5.137*
θ_{5_H}	128.(5)	130.(5)	128.(5)	124
	R = 5.712	R = 5.676	R = 5.666	R = 5.760

[a] The values of the coordination numbers were fixed to the theoretical values $N_1 = 4$, $N_2 = 2$. $N_3 = 2$ and $N_1 = 2$, $N_2 = 2$, $N_3 = 2$, $N_3 = 6$ for Bixbiyte and Hausmannite, respectively. S_0^2 was fixed to 0.74. Distances in Å, Debye−Waller factors in $Å^2$, angles in degrees. The errors of the fitting parameters are reported in parentheses.

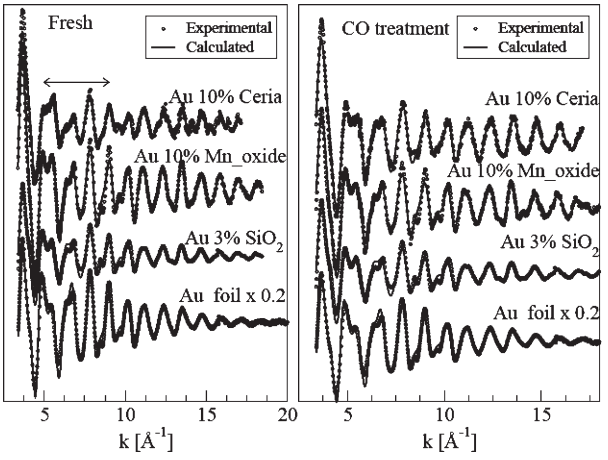

Figure 4. EXAFS signal on the L_{III} Au-edge of the ceria and manganese gold catalysts. Left panel shows the "as-prepared samples". In the right panel are reported the extracted signal after CO treatment. Gold silica catalyst and the Au foil are also shown. The arrow shows the *k* range where the Au−O component influences the EXAFS signal.

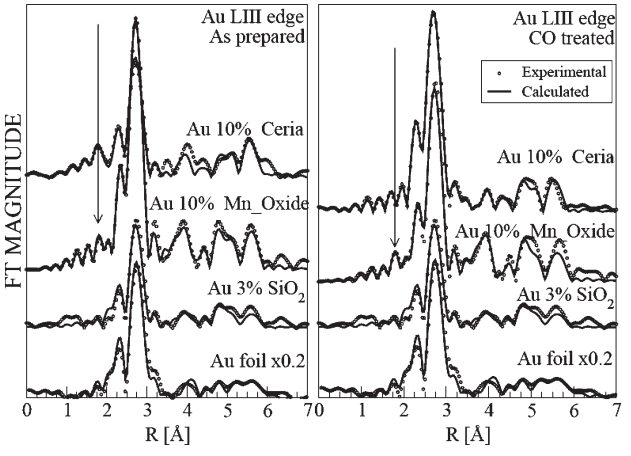

Figure 5. Fourier transform (uncorrected for phase shift) magnitude of the experimental data (circles) and of the calculated EXAFS signals (line) shown in Figure 4. The arrows are a visual guideline indicating the position of the Au−O contribution.

FT transform, not observed in the silica supported catalyst, is well-evident in both manganese oxide and ceria-based samples. This component can also be clearly recognized in the analysis of the catalysts reduced by CO treatment, validating the hypothesis of SMSI occurrence. In Table 5 the calculated gold cluster size is also listed. In both "as-prepared" manganese and cerium oxide supported gold catalysts, the calculated Au particle size is 32(5) Å and 45(5) Å respectively.[42] An increase in the mean diameter occurred after CO treatment, to a large extent of metal content in the Au (10 wt %)/γ-MnO_2. However, such structural change did not affect the extent of Au−O interaction which is similar to the as prepared catalyst, confirming the presence of gold clusters strongly interacting with the support. The XRD particle size is larger than the size obtained with the EXAFS analysis. This is not surprising, because XRD is sensitive to the square volume of the scattering objects, so that the smaller metal clusters give a negligible contribute to the pattern. On the contrary, EXAFS is sensitive to interatomic distances between all the atoms in the sample, so that all the particles give an important contribution to the signal, regardless of their size. As concerns the ceria-supported catalyst, the value of the Au−O distance is in agreement with previous results reported by other authors and is indicative of a covalent bonding between the supported gold clusters and the oxygen atoms of nanocrystalline ceria.[43−45] To the best of our knowledge, it is the first time that the value of 2.1 Å for the Au−O

(42) Borowski, M. *J. Phys. IV* (*Paris*) **1997**, *7*, C2-259–260.

(43) Carrettin, S.; Hao, Y.; Aguilar-Guerrero, V.; Gates, B. C.; Trasobares, S.; Calvino, J. J.; Corma, A. *Chem.—Eur. J.* **2007**, *13*, 7771–7779.

(44) Deng, W.; Frenkel, I. A.; Si, R.; Flytzani-Stephanopoulos, M. *J. Phys. Chem. C* **2008**, *112*, 128.

(45) Argo, A. M.; Odzak, J. F.; Lai, F. S.; Gates, B. C. *Nature* **2002**, *415*, 623–626.

Table 5. EXAFS Analysis Relative to Au L_{III}-Edge of CO-Treated Samples.[a]

Au L_{III}-edge Parameters	as-prepared 10 wt % Au/γMnO_2	CO-treated 10 wt % Au/γMnO_2	as-prepared 10 wt % Au/Ceria	CO-treated 10 wt % Au/Ceria	theoretical values
E_0	11 921.(2)	11 920.(2)	11 920.(2)	11 921.(2)	11 920
N1	11.7	11.9	10.5	11.9	12
N2	5.8	5.9	4.9	6.0	6
N3	23.0	23.7	18.7	23.8	24
N4	11.4	11.8	8.9	11.9	12
R1	2.865(5)	2.868(5)	2.855(5)	2.859(5)	2.890
σ_1	0.0027(3)	0.0029(2)	0.0037(5)	0.0032(5)	
D (cluster size) (Å)	37.(10)	120.(10)	24.(10)	42.(10)	
R_2	4.051(5)	4.056(5)	4.036(5)	4.043(5)	4.087
σ_2	0.0034(5)	0.0025	0.0043	0.0067	
θ_1	120.	120.	121.	121.	120.
	R = 4.993	R = 4.994	R = 4.990	R = 4.993	R = 4.995
θ_2	180	180	180	180	180
	R = 5.736	R = 5.751	R = 5.736	R = 5.738	R = 5.760
$N\__{OX}$	0.3(5)	0.1(5)	0.2(5)	0.1(5)	
$R\__{OX}$	2.093(6)	2.096	2.066	2.068	
σ_{2_OX}	0.0046(7)	0.001(7)	0.0036(7)	0.0026(7)	

[a] The errors of the fitting parameters are reported in parentheses. In bold case are reported the parameters used in the fitting procedure. The parameters used in the fitting procedure are reported in bold case.

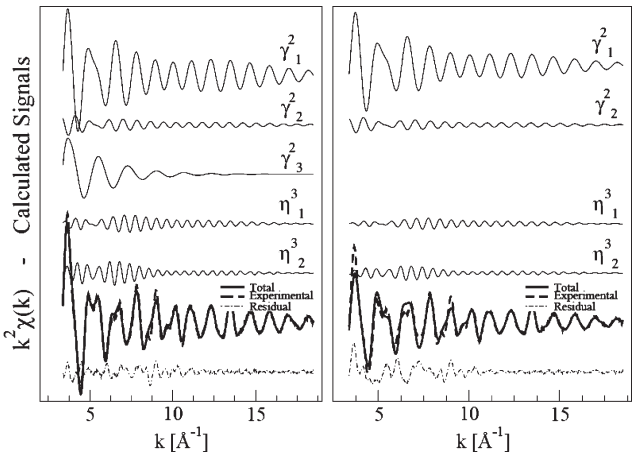

Figure 6. Component signals and overall fitting to the EXAFS data. Two-body components are indicated by γ_i^2 and three-body components by η_i^3. The left panel shows the EXAFS analysis including the Au−O component. The result without the Au−O component is shown in the right panel.

distance is reported for gold supported on manganese oxide.

3.5. XPS Analysis. In order to detect the surface oxidation state and chemical composition, XPS analyses of the "as-prepared" and of the CO-treated samples were performed. The XPS results for the precursor Mn oxide (sample A), for the as prepared γ-MnO_2 (sample B) and for the as prepared Au(10 wt %)/γ-MnO_2 catalyst are summarized in Table 6. Moreover, data referred to the samples treated with 1%CO/He at 250 °C for 90 min are also enclosed. The Au $4f_{7/2}$, the Mn $2p_{3/2}$, and the average Mn 3s binding energies along with the Mn 3s multiplet splitting and with the atomic percentage of gold, Au (at %), and O/Mn atomic ratios are listed. The corresponding Mn 3s spectra are shown in Figure 7A−C. The Au 4f doublet overlaps with the Mn 3s multiplet splitting peaks from the support. However, by curve fitting procedure, assuming for the gold-containing samples the same Mn 3s/Mn 2p intensity ratio as for the bare MnO_2 and constraining the relative position and intensity of the two Au $4f_{7/2}$ and Au $4f_{5/2}$ components to the expected values of 3.6 eV and 1.33, respectively, the peak position and area of the Au 4f doublet was obtained.[41] Because the relative intensity and position of the Mn 3s splitting peaks are strongly dependent on the coordination structure of the manganese compounds, the weighted average of the two components is considered to reflect more reliably the oxidation state of manganese.[46] The average Mn3s binding energies reported in Table 6 were calculated from the peak positions and their integral areas. In Figure 7 are shown the Mn 2p spectra of the γ-MnO_2 before and after the CO treatment. The $Mn2p_{3/2}$ binding energy value of 642.0 eV obtained for the pure support is in agreement with literature data.[47−50] After CO treatment the binding energy of the main Mn $2p_{3/2}$ photoelectron peak is down shifted to value of 641.3 eV typical of Mn_3O_4.[49] The gold containing samples, before and after CO treatment are always characterized by the Mn $2p_{3/2}$ photoelectron peak close to the value obtained from the reduced MnO_2. Similar trend is observed for the average Mn 3s binding energies. Concerning the O/Mn atomic ratios, an excess of oxygen is obtained in both cases, in the oxidized samples (2.4 instead of the stoichiometric 2) and in the reduced samples (2 rather than 1.33 or 1.5 as expected for Mn_3O_4 or Mn_2O_3). According to Galakhov et al. the energy difference (ΔE) between the two Mn3s components relates to the average oxidation state (AOS) through the relationship AOS = 8.956−1.126(ΔE).[50] In Table 6, the so-obtained AOS values of the manganese are also reported. The AOS = 3.3 for sample B is in accord with the presence of a reduced manganese in the supposedly

(46) Pena, D. A.; Uphade, B. S.; Sminiotis, P. G. *J. Catal.* **2004**, *221*, 421.
(47) Wang, L. C.; Liu, Y. M.; Chen, M.; Cao, Y.; He, H. Y.; Fan, K. N. *J. Phys. Chem. C* **2008**, *112*, 6981.
(48) Lee, S. J.; Avriilidis, A. G.; Pankhurst, Q. A.; Kyek, A.; Wagner, P. F. E.; Wong, C. L.; Yeung, K. L. *J. Catal.* **2001**, *200*, 298.
(49) Carver, J.; Schweitzer, G. K.; Carlson, T. A. J. *Chem. Phys.* **1972**, *57*, 973.
(50) Galakhov, V. R.; Demeter, M.; Bartkowski, S.; Neumann, M.; Ovechkina, N. A.; Kurmaev, E. Z.; Lobachevskaya, N. I.; Mukovskii, Y. M.; Mitchell, J.; Ederer, D. L. *Phys. Rev. B* **2002**, *65*, 1131021–11311024.

Table 6. XPS Results: Binding Energy of Au $4f_{7/2}$, Mn $2p_{3/2}$, Mn 3s (average); Mn 3s Splitting (ΔE), O/Mn Atomic Ratio, Au Atomic Percentage, And Average Oxidation State (AOS) of Mn

sample	Au4f $_{7/2}$ (eV)	Mn 2p $_{3/2}$ (eV)	avg Mn 3s (eV)	ΔE (Mn3s) (eV)	O/Mn	Au (at %)[b]	AOS
A		641.3	85.5	5.4	1.8		2.9
B		642.0	86.3	5.0	2.4		3.3
D[a]		641.3	85.5	5.5	2.0		2.7
10 wt %Au/γ-MnO_2 as-prepared	84.4	641.6	86.0	5.4	2.0	0.4	2.8
10 wt %Au/γ-MnO_2 CO-treated (sample E)	84.4	641.5	86.1	5.7	2.0	0.4	2.5

[a]Sample D is sample B after CO treatment at 250 °C. [b]The analytical Au (at %) determined by ICP-AES technique is 1.4.

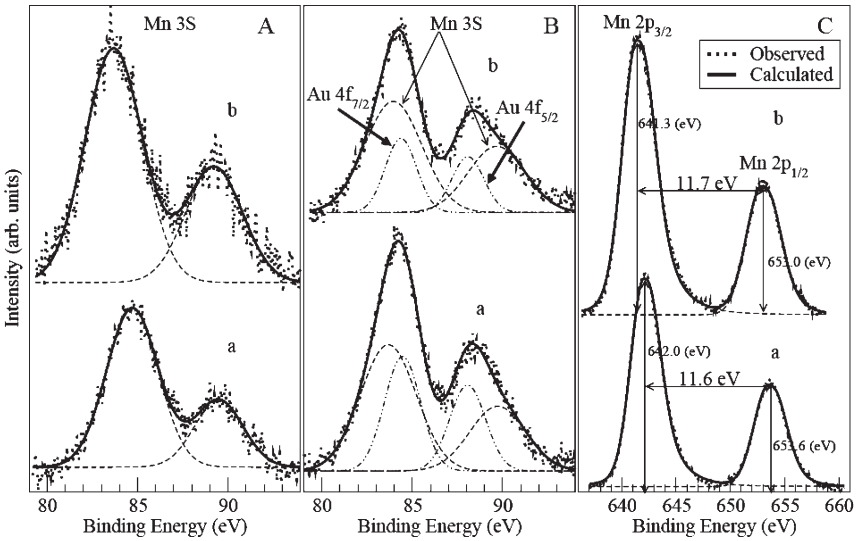

Figure 7. (A) Mn 3s spectra of γ-MnO_2: (a) before reduction (sample B); (b) after reduction (sample D). (B) Mn 3s and Au 4f XP spectra of Au10 wt %/γ-MnO_2: (a) as-prepared; (b) after CO treatment (sample E). (C) Mn2p spectra of γ-MnO_2: (a) before reduction (sample B); (b) after reduction (sample D).

pure γ-MnO_2 and AOS = 2.7 is in accord with the presence of Mn_3O_4 in the reduced sample. Again, the gold catalyst is characterized by reduced manganese in the as-prepared sample (AOS = 2.8) and by more reduced manganese after the CO treatment (AOS = 2.5). The Au 4f binding energy of 84.4 eV, detected in both samples, the "as-prepared" and the "CO-treated" Au 10 wt % catalyst, is typical of metallic gold. Moreover, as seen in Table 6, the XPS-derived gold amount present at the surface sample is much less (0.4 at %) with respect to the analytical amount (1.4 at %).

5. Discussion

The EXAFS results performed on Mn K-edge pointed out that from the structural point of view, the support reduction process is sensitive to the metal content. Supported also by the XPS data, the presence of gold promotes the reduction of MnO_2 and such effect is particularly pronounced for Au(10 wt %). Accordingly, the CO treatments have different effect on the gold catalysts (1 and 10 wt %) and on the bare support (see the Supporting Information).[51]

It is widely accepted that CO oxidation over manganese oxides proceeds via the Mars-van-Krevelen mechanism which involves the reaction of adsorbed CO with the labile lattice oxygen.[52] The reactivity is attributed to the capacity of manganese to adopt various oxidation states, e.g., Mn^{2+}/Mn^{3+} or Mn^{3+}/Mn^{4+}, and oxygen mobility in the oxide lattice. In this respect, the addition of gold can have a notable influence on the redox properties of the manganese oxide supports. It was reported that the presence of gold particles promotes the reduction of the support, enhancing the mobility of lattice oxygen by modifying the rate of vacancy exchange between the bulk and the oxide surface.[53] According to the mechanism proposed by Sinha et al. for the oxidation of VOCs, the efficiency of gold deposited on mesoporous γ-MnO_2 is due to the interaction of the support with the metal particle, which induces an increase of the oxygen vacancies.[35] The results obtained on the Au L_{III} edge are in agreement with a strong interaction between gold clusters and manganese oxide. The Au−O bonding suggests that the positive Au cation constitutes an interface located between the clusters and the support, as already suggested in previous work.[30−36] The Au−O contribution is detectable also after the reducing treatment, so that gold remains strongly interacting with the support. The disagreement between EXAFS and XPS results, which detect essentially metallic gold, is explained by the different probing depths of the two techniques. XPS reflects the average chemical state within about 6 nm from the surface, whereas the EXAFS technique probes each different

(51) Longo, A.; Liotta, L. F.; Giannici, F.; Di Carlo, G; Pantaleo, G.; Venezia, A.; Martorana, A. **2010**, in preparation.
(52) Ramesh, K.; Chen, L.; Che, F.; Liu, Y.; Wang, Z.; Han, Y.-F. *Catal. Today* **2008**, *131*, 477.
(53) Wang, L.; Liu, Q.; Huang, X.-S.; Liu, Y.-M.; Cao, Y.; Fan, K.-N. *Appl. Catal., B* **2009**, 204–212.

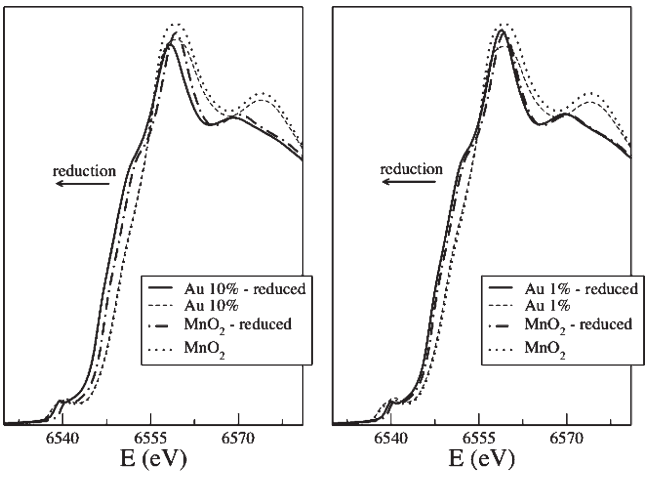

Figure 8. XANES spectra for as-prepared and reduced manganese oxide supports, and gold catalysts.

local environment of gold regardless how deep the gold particles are inside the sample. Furthermore, in spite of the large amount of metal loaded on the support (10% weighted), the XPS analysis performed in the fresh and reduced samples detected only a small amount of Au species on the surface suggesting, in agreement with the literature data, that the small gold clusters are covered by the support and embedded in the manganese oxide.[36] On the contrary, as witnessed by the XPS result, the larger metal particles are stabilized at the support surface.

For comparison, we report the structural results of gold clusters dispersed in ceria. Also in this case the Au−O component is needed to obtain a satisfactory agreement between the experimental and calculated EXAFS signal.[16,30,53] Recently, Andreeva et al., in a XPS study of ceria/alumina gold catalysts, proposed that the complex $Au^{\delta+}V_oCe^{3+}$ exists in the fresh catalysts, where V_o stands for oxygen vacancy. This indicates a strong modification of the support with formation of oxygen vacancies, which enhances the electron transfer between defective ceria and partially charged gold particles via oxygen vacancies, improving the activity of the catalyst.[30] The present results support this interaction. Similar results, in which the presence of defects is located near the interfaces between the gold clusters and the support, were obtained by Carrettin and co-workers for a gold catalysts dispersed on iron doped titania.[43]

No evidence of metal−support interaction were found for gold over inert silica. On the basis of these observations, it is possible to suppose that also for the gold catalysts dispersed on the manganese oxide, the interaction between gold nanoclusters and the support occurs via oxygen vacancies by formation of a complex of Au partially charged with the oxygen vacancies. This mechanism is corroborated by the XANES spectra collected at the Mn K-edge (Figure 8), which show an edge shift in the samples containing gold metal clusters, in agreement with a more reduced phase.[34] On the other hand, the oxygen vacancies are already present in the nanostructured metal-free manganese oxide and they increase when the gold is loaded and dispersed on the support.[34] Moreover DFT calculation showed that the vacancies are confined in the vicinity of the metal particles and stabilized by the Au partially charged clusters, acting as anchoring sites for gold nanoclusters nucleation.[55] A gradient of vacancy concentration is then established between the bulk and the surface of the oxide where the gold clusters are mainly localized. It is likely that this gradient promotes the migration of bulk oxygen and the formation of reactive species like a superoxide or peroxide species toward the surface near the sites of the metal clusters.[43] Furthermore, as previously shown, the oxidation of CO occurs on the metal sites, and this process facilitates the spillover of more reactive oxygen in the clusters surface where the CO is adsorbed.[43,54]

6. Conclusion

In this work, we report a detailed analysis of the EXAFS spectra at the Mn K-edge and Au L_{III}-edge of gold catalysts dispersed in γ-MnO_2 oxide. The EXAFS results on the fresh support indicated and put in evidence that the treatment with sulphuric acid promotes the oxidation of the Hausmannite (Mn_3O_4) to γ-MnO_2 leaving some amorphous Mn_3O_4. The CO treated samples are characterized by the presence of Hausmannite and Bixbyite (Mn_2O_3) phases. Increasing the gold loading increases the Hausmannite fraction, which is the more reduced phase. Moreover, the beneficial effect of gold in promoting γ-MnO_2 reduction is more pronounced in the Au(10 wt %) catalyst, which exhibits a superior CO oxidation activity, with respect to Au(1 wt %) and the metal free oxide. The higher efficiency of Au(10 wt %) catalyst, in spite of the large Au particle size, is attributable to the strong metal support interaction between gold and support giving rise to peculiar reactivity properties.

For the first time, by EXAFS analysis, similarly to the CeO_2-supported gold catalyst, a component Au−O is reported at 2.1 Å also for the γ-MnO_2 gold catalysts. The result suggests that the interaction between gold nanoclusters and the γ-MnO_2, similarly to the ceria-supported catalysts, occurs via oxygen vacancy formation, in agreement with the literature. Moreover, the correlation between the structural changes of the CO treated catalysts and the CO oxidation profiles suggest a mechanism of support reduction, which involves a gradient of oxygen vacancies. This gradient promotes the migration of bulk oxygen species toward the surface near the gold nanoclusters, where CO oxidation occurs, maintaining a high CO conversion for a longer time.

Acknowledgment. Support by ELETTRA Synchrotron Light Laboratory (Trieste, Italy), proposal number 2008322, by European Community, Network of Excellence (NoE) IDECAT (Integrated Design of Catalytic Nanomaterials for Sustainable Production) and COST D36 action is acknowledged.

Supporting Information Available: Additional figures and information (PDF). This material is available free of charge via the Internet at http://pubs.acs.org.

(54) Zhang, C.; Michaelides, A.; King, D. A.; Jenkins, S. J. *J. Phys. Chem. C* **2009**, *113*, 6411–6417.

(55) Prestianni, A.; Martorana, A.; Labat, F.; Ciofini, I.; Adamo, C. *J. Phys Chem. C* **2008**, *112*, 18061.